EDGE ARTICLE

Non-covalent S···O interactions control conformation in a scaffold that disrupts islet amyloid polypeptide fibrillation†

Hayden Peacock,[a] Jinghui Luo,[a] Tohru Yamashita,[a] James Luccarelli,[a] Sam Thompson,*[a] and Andrew D. Hamilton*[ab]

Conformationally-constrained molecules that selectively recognise the surfaces of proteins have the potential to direct the path of protein folding. Such molecules are of therapeutic interest because the misfolding of proteins, especially that which results in fibrillation and aggregation, is strongly correlated with numerous diseases. Here we report the novel use of S···O interactions as a conformational control element in a new class of non-peptidic scaffold that mimics key elements of protein surfaces. These molecules disrupt the fibrillation of islet amyloid polypeptide (IAPP), a process that is implicated in the pathology of type II diabetes.

Introduction

Correctly folded proteins have myriad roles critical for life, including structural support, signal mediation and catalysis. Conversely, misfolded forms are associated with numerous diseases, including neurodegenerative disorders such as Alzheimer's and Parkinson's, and non-neuropathic conditions such as type II diabetes.[1] The use of small molecules to mediate aberrant protein folding is a hugely appealing therapeutic strategy,[2–4] however there are few rationally designed examples. A potential solution is the use of protein surface mimetics that modulate the energy landscape of protein folding *via* selective recognition of complementary protein surfaces, analogous to nature's chaperone proteins. Work by our group and others has established several families of synthetic protein surface mimetics that reproduce key recognition features of protein secondary structure[5–9] and can thereby affect the pathways of protein folding.[10,11]

In order to maximise target-binding affinity, protein surface mimetics are based on conformationally pre-organised scaffolds. This increases the population of the desired conformer and thus reduces the entropic cost of binding. Previous non-peptidic scaffolds have taken advantage of hydrogen bonding,[12–16] the stereoelectronic preferences of secondary aryl amides,[13,17,18] steric repulsion between vicinal cyclic systems,[19,20]

[a]*Chemistry Research Laboratory, University of Oxford, 12 Mansfield Road, Oxford, OX1 3TA, UK. E-mail: sam.thompson@chem.ox.ac.uk; Tel: +44 (0) 1865 275978*
[b]*Department of Chemistry, New York University, New York, New York 10003, USA. E-mail: andrew.hamilton@nyu.edu*

† Electronic supplementary information (ESI) available: Experimental procedures; ^{1}H, ^{13}C and NOESY spectra; HRMS, and IR values. CCDC 1453550 (**24**). ThT assay data, computation, electron microscopy. For ESI and crystallographic data in CIF or other electronic format see DOI: 10.1039/c6sc00756b

dipolar repulsion,[21,22] cyclisation,[23] and metal templation[24] to provide conformational pre-organisation (Fig. 1).

With the aim of expanding the toolkit of scaffolds for protein surface mimicry we set out to explore additional conformational determinants that promote pre-organisation. The S···O
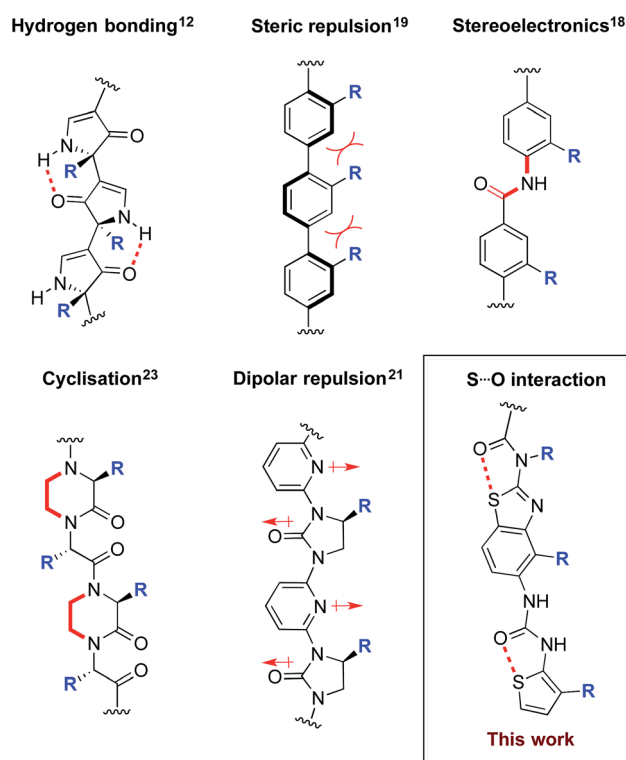

Fig. 1 Conformational determinants of non-peptidic protein surface mimetics.
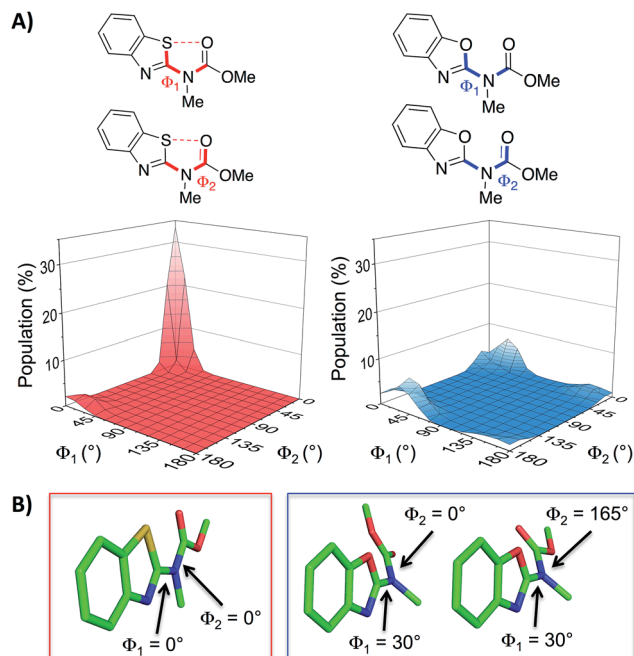
Fig. 2 (A) Dihedral contour plots of a model system depicting the difference in conformational preference between benzothiazole and benzoxazole rings. The relevant dihedral angles are depicted in bold and the plots show the Boltzmann population of conformers at 298 K. (B) The model systems displayed in their most highly populated conformations (benzothiazole system in the red box and benzoxazole system in the blue box, see also the ESI†). The calculations were performed at the M06-2X/6-31G(d,p) level of theory with implicit aqueous solvent.[29–34]†

interaction involves a low-lying C–S σ* molecular orbital that accepts electron density from an adjacent oxygen lone pair.[25–27] Many observations of this effect have been made *ex post facto* – frequently upon inspection of X-ray diffraction data. However, there are few examples in which the interaction is incorporated as a conformational determinant of rationally designed compounds. The effect of the S⋯O interaction is highlighted by quantum mechanical simulation of a benzothiazole model system in which population distribution is evaluated as a function of two key dihedral angles (Φ_1 and Φ_2, Fig. 2A). A 1,5-S⋯O interaction heavily biases the conformation towards one in which the sulfur and oxygen atoms are co-planar and adjacent to each other (Φ_1 and Φ_2 of 0°, Fig. 2B), with a barrier to rotation about Φ_1 of 7.4 kcal mol^{-1} when Φ_2 is constant at 0°. In contrast, a model system containing an oxygen atom in place of sulfur is less biased towards a single conformation, and has an approximately equal preference for two out-of-plane geometries (Fig. 2B).[28]

Here we explore the 1,5-S⋯O interaction as a determinant of conformation in a benzothiazole–thiophene scaffold. This scaffold projects three substituents (R^2, R^3, R^4) that mimic the *i*, *i* + 3/4 and *i* + 7 side-chains vectors of one face of an α-helix.

Results and discussion

The synthesis began with the preparation of 5-nitrobenzo[*d*]thiazol-2-amine **1** on a multi-gram scale from 2-fluoro-5-

nitroaniline in two steps.[35]† A range of R^1 and R^2 groups were introduced either by *N*-acylation and *N*-alkylation (Scheme 1, Route 1), or an alternative sequence in which the amine was diazotized and substituted with chlorine, allowing introduction of substituted amines by nucleophilic substitution followed by *N*-acylation (Scheme 1, Route 2).† Reduction of the aromatic nitro group of compounds **5–7** with hydrogen under palladium on carbon catalysis gave anilines that were regioselectively
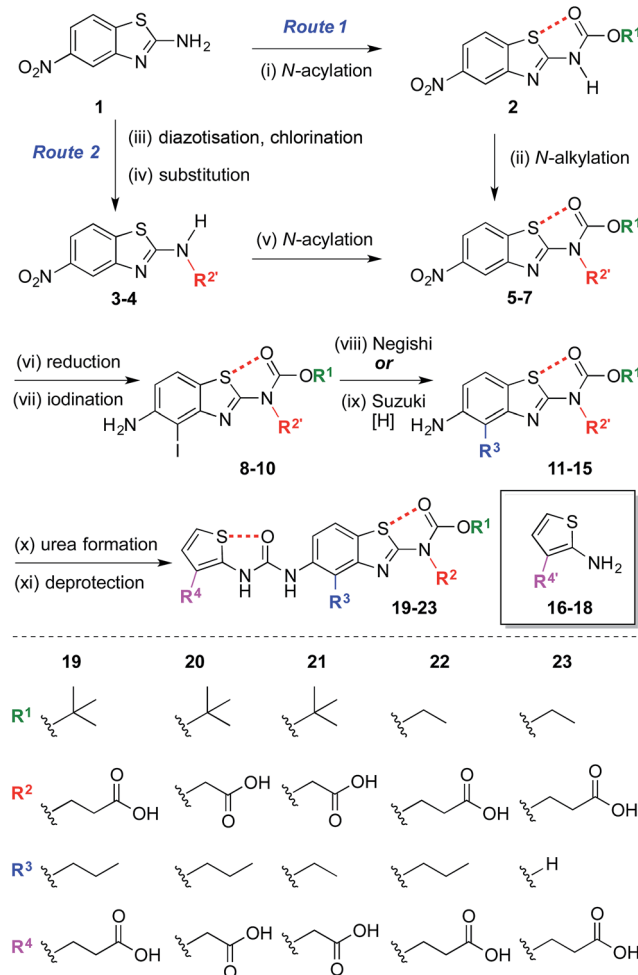
Scheme 1 Modular synthesis of protein surface mimetics stabilised by 1,5-S⋯O interactions. Reagents and conditions: (i) Boc$_2$O, DMAP, DMF, 60 °C, 4 h, 47%; (ii) NaH, BrCH$_2$CO$_2$Me, DMF, 0 °C – r.t., 1 h, 69%; (iii) *i*-BuONO, CuCl$_2$·H$_2$O, MeCN, r.t. – 60 °C, 1 h; (iv) NH$_2$R$^{2'}$, *i*-Pr$_2$NEt, DMF, r.t., 16 h, 41–51% over two steps; (v) (CO$_2$Et)$_2$O, DMAP, MeCN, 1 h, r.t., 92%; (vi) H$_2$, Pd/C, THF–MeOH, r.t., 1.5–4 h, 74–85%; (vii) NIS, MeCN, 0 °C – r.t., 10–30 min, 84–99%; (viii) *n*-PrMgCl, ZnCl$_2$, PdCl$_2$(dppf), THF, 65 °C, 2 h, 14–35%; (ix) H$_2$CCHBF$_3$K, PdCl$_2$(dppf), Et$_3$N, EtOH, 70 °C, 3 h, then H$_2$, Pd/C, THF–MeOH, r.t., 30 min, 42% over two steps; (x) **16–18**, COCl$_2$, Et$_3$N, CH$_2$Cl$_2$, 0 °C, 30 min, then Et$_3$N, CH$_2$Cl$_2$, aniline **11–15**, r.t., 1 h, 17–78%; (xi) Me/Et ester: NaOH, THF–MeOH, r.t. – 60 °C, 1 h, 33–59%; allyl ester: piperidine, Pd(PPh$_3$)$_4$, THF, r.t., 30 min, 44%; *t*-Bu ester: TFA, CH$_2$Cl$_2$, r.t., 30 min, 96%.† *n* = normal, Boc = CO$_2$*t*-Bu, DMAP = 4-dimethylaminopyridine, DMF = *N*,*N*-dimethylformamide, Me = methyl, Bu = butyl, Pr = propyl, THF = tetrahydrofuran, NIS = *N*-iodosuccinimide, dppf = bis(diphenylphosphino)ferrocene, Et = ethyl, Ph = C$_6$H$_5$, TFA = trifluoroacetic acid. R′ denotes a carboxylic acid side-chain protected as an ester [Me, Et, allyl, or *t*-Bu].†

iodinated to give **8–10**. Negishi or Suzuki cross-coupling allowed introduction of various R^3 groups followed in the latter case by hydrogenation of the resultant alkene. A range of thiophene ureas, and thus R^4 groups, were introduced via nucleophilic attack of anilines **11–15** on isocyanates formed in situ from 2-amino thiophenes **16–18** with phosgene.

2D NOESY data acquired on mimetic **20** are consistent with population of the desired conformation in the solution phase (Fig. 3A). Substituents R^2 and R^3 of **20** are separated by approximately 5 Å in the desired conformation. This separation is greater in all other conformations and is a maximum of approximately 6.5 Å if an anti-arrangement of these groups is adopted. Since 5 Å is the accepted cut-off distance for an observable nOe in a non-flexible system,[36] the presence of an nOe correlation between the hydrogens of these substituents indicates that the desired conformation is likely to be a significant contributor to the solution phase conformational ensemble.

The X-ray crystal structure of iodide **24**, an analogue of **19–23**, confirms the presence of two 1,5-S···O interactions (Fig. 3B).† There is planarity about both the carbamate–benzothiazole and urea–thiophene units, and the S···O distances are 2.7 Å and 2.9 Å, respectively, smaller than the sum of the van der Waals radii of sulfur and oxygen (3.3 Å). The projection of three substituents (R^2, R^3 and R^4) is in good agreement with sidechains i, $i + 4$ and $i + 7$ of a canonical α-helix (Fig. 3C). This positioning is analogous to the previously reported oligopyridylamide and oligobenzamide scaffolds.[10,13] A six-point RMSD

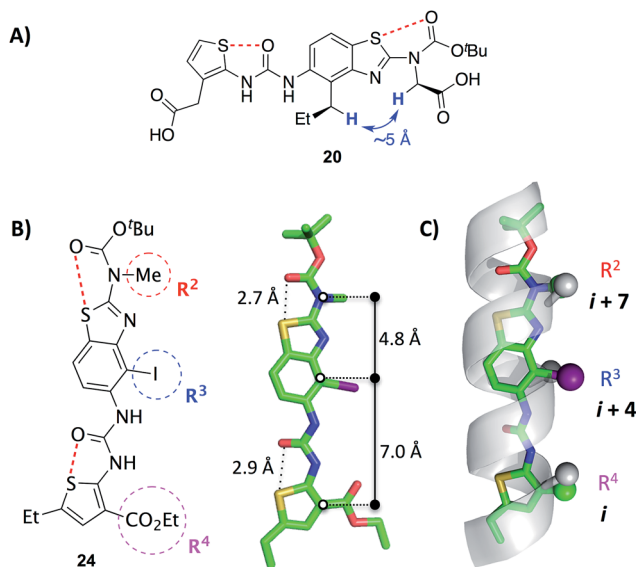of 1.4 Å was calculated from the superposition of three α-carbons and three β-carbons of the α-helix with the corresponding atoms of the scaffold.[37]

In order to assess the capacity of the benzothiazole–thiophene scaffold to act as a protein surface mimetic, we studied the ability of appropriately functionalised variants to disrupt the fibrillation of islet amyloid polypeptide (IAPP). The self-association of intrinsically-disordered 37-residue IAPP (Fig. 4A) ultimately leads to amyloid fibrils (highly-ordered β-rich aggregates) which are the main component of the protein deposits in the pancreatic islets of type II diabetes patients.[38,39] In the presence of phospholipid membranes_– such as those found within biological systems_– the N-terminus of IAPP (residues 5–22) populates α-helical states before undergoing fibrillisation (Fig. 4B).[40,41] The stabilisation of these membrane-bound α-helical states attenuates the formation of IAPP fibrils[41] and, as recent evidence suggests, decreases the cellular toxicity of IAPP.[41,42] This indicates therapeutic applications of IAPP helix stabilisers. In our previous work, scaffolds functionalised with acidic, hydrophobic and acidic groups that overlay with positions i, $i + 3/4$ and $i + 7$ of an α-helix, respectively, were highly effective disruptors of membrane-catalysed IAPP fibrillation.[10,11,42] These surface mimetics were complementary to sidechains of the α-helical N-terminus of IAPP (postulated to be Arg11, Asn14/Phe15 and His18) and stabilised its helix formation (Fig. 4C).[42]

We measured the fibrillation of IAPP using a thioflavin T (ThT) assay[43] in the presence of a model membrane system.[44] The fluorescence intensity of ThT correlates with the extent of protein fibril formation. The assay confirmed that ability of the benzothiazole–thiophenes to disrupt the fibrillation of IAPP. This can be seen by the lower end-point fluorescence intensity of the samples containing **19**, **22** and **23** relative to the IAPP control (Fig. 5A). Additionally, the IAPP fibrillation process is delayed in the presence of these three compounds in comparison to control, seen by the extended times to half-maximal fibrillation ($t_{1/2}$) of these samples (Fig. 5B). The results of the ThT assay were confirmed by electron microscopy, which showed that treatment of IAPP with **19** and **22** gives rise to amorphous aggregates whereas **21** gives rise to a combination of amorphous aggregates and ordered fibrils (ESI Fig. 3†). Furthermore, circular dichroism (CD) confirmed that compound **19** disrupts the transition of IAPP from its initial α-helical conformation (a spectrum characterised by two
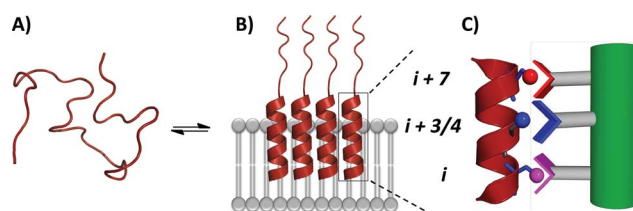

Fig. 3 (A) A key ^1H homonuclear nOe correlation observed in **20** (solution in d_6-DMSO). The distance between the highlighted hydrogens is approximately 5 Å in the desired conformation.† (B) X-ray crystal structure of the benzothiazole–thiophene scaffold **24**.† The solid lines indicate the distances between the atoms on the scaffold that superimpose with the α-carbons at positions i, $i + 4$ and $i + 7$ of a canonical α-helix. The red dashed lines indicate the 1,5-S···O interactions. (C) Superposition of the scaffold with a canonical α-helix (residues 19–31 of pdb 1HLO). The β-carbons of the helix and corresponding atoms of the scaffold are shown as spheres. The ethyl-carboxy substituent of the scaffold (R^4) is truncated for clarity.

Fig. 4 (A) IAPP is intrinsically disordered in solution. (B) IAPP populates α-helical states in the presence of a lipid membrane. (C) α-Helical states are targets for surface-mimetics that form complementary interactions with side-chains of the protein.
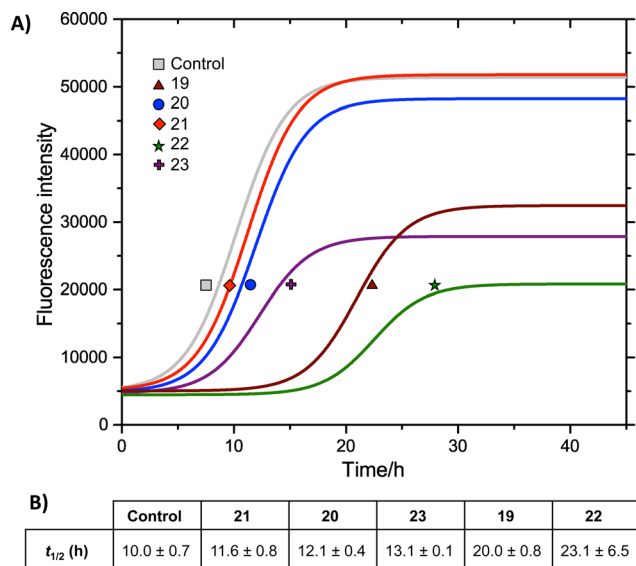
Fig. 5 (A) ThT fibrillation kinetics of 10 μM IAPP in the absence (grey curve) or presence of 50 μM test compounds. Each curve represents the average of six replicates. (B) Times to half-maximal fibrillation ($t_{1/2}$). Conditions: 500 μg mL^{-1} DOPG/DOPC liposomes (1 : 1), 20 mM potassium phosphate buffer, 100 mM sodium chloride, pH 7.2, 25 °C.†

minima at 208 and 222 nm) to a β-sheet conformation (a spectrum characterised by a single minimum at approximately 215 nm) in the presence of a model membrane system (Fig. 6).

The most striking feature of the structure–activity relationship is that the active compounds bear three-carbon carboxylic acid substituents at positions R^2 and R^4, however the inactive compounds, **20** and **21**, both bear two-carbon carboxylic acids substituents at these positions. This indicates that the length of the acidic substituents at positions R^2 and R^4 is critical to the interaction between the protein and the small molecule,
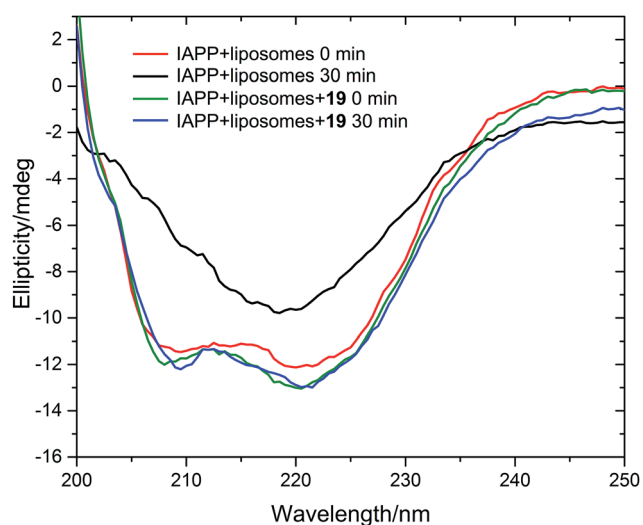

Fig. 6 Circular dichroism spectra of IAPP in the absence (red and black curves) and presence (green and blue curves) of **19**. Conditions: 20 μM IAPP, 20 μM **19**, 1 m g mL^{-1} DOPG/DOPC liposomes (1 : 1), 20 mM potassium phosphate buffer, 100 mM sodium chloride, pH 7.2, 25 °C.

consistent with the formation of specific contacts. The central hydrophobic substituent (R^3) was also sensitive to modification. Compound **23**, which differs from **22** only by the absence of this central substituent, was a less effective inhibitor of fibrillation. This is consistent with a previous observation that the central hydrophobic substituent is sensitive to modification within an oligopyridylamide scaffold displaying an analogous set of functional groups.[43]

Conclusions

We have synthesised a new non-peptidic protein surface mimetic based on a benzothiazole–thiophene scaffold that is conformationally pre-organised by two 1,5-S⋯O interactions. The scaffold directs three side-chains to positions i, $i + 3/4$ and $i + 7$ of an α-helix. The S⋯O interaction was evaluated as a determinant of conformation by calculation, X-ray crystallography and solution-phase NMR spectroscopy. A focussed library of conformationally constrained scaffolds displaying a range of functional groups act as protein surface mimetics that disrupt membrane-catalysed islet amyloid polypeptide (IAPP) fibrillation, a pathway strongly associated with the pathology of type-II diabetes.

Acknowledgements

Notes and references

1 T. P. J. Knowles, M. Vendruscolo and C. M. Dobson, *Nat. Rev. Mol. Cell Biol.*, 2014, **15**, 384–396.

2 L. K. Gavrin, R. A. Denny and E. Saiah, *J. Med. Chem.*, 2012, **55**, 10823–10843.

3 L. M. Young, J. C. Saunders, R. A. Mahood, C. H. Revill, R. J. Foster, L.-H. Tu, D. P. Raleigh, S. E. Radford and A. E. Ashcroft, *Nat. Chem.*, 2015, **7**, 73–81.

4 G. Tóth, S. J. Gardai, W. Zago, C. W. Bertoncini, N. Cremades, S. L. Roy, M. A. Tambe, J.-C. Rochet, C. Galvagnion, G. Skibinski, S. Finkbeiner, M. Bova, K. Regnstrom, S.-S. Chiou, J. Johnston, K. Callaway, J. P. Anderson, M. F. Jobling, A. K. Buell, T. A. Yednock, T. P. J. Knowles, M. Vendruscolo, J. Christodoulou, C. M. Dobson, D. Schenk and L. McConlogue, *PLoS One*, 2014, **9**, e87133.

5 V. Azzarito, K. Long, N. S. Murphy and A. J. Wilson, *Nat. Chem.*, 2013, **5**, 161–173.

6 M. K. P. Jayatunga, S. Thompson and A. D. Hamilton, *Bioorg. Med. Chem. Lett.*, 2014, **24**, 717–724.

7 A. M. Watkins and P. S. Arora, *Eur. J. Med. Chem.*, 2015, **94**, 480–488.

8 D. Xin, A. Raghuraman and K. Burgess, *J. Org. Chem.*, 2015, **80**, 4450–4458.

9 M. Oh, J. H. Lee, W. Wang, H. S. Lee, W. S. Lee, C. Burlak, W. Im, Q. Q. Hoang and H.-S. Lim, *Proc. Natl. Acad. Sci. U. S. A.*, 2014, **111**, 11007–11012.

10 I. Saraogi, J. A. Hebda, J. Becerril, L. A. Estroff, A. D. Miranker and A. D. Hamilton, *Angew. Chem., Int. Ed.*, 2010, **49**, 736–739.

11 O. V. Kulikov, S. Kumar, M. Magzoub, P. C. Knipe, I. Saraogi, S. Thompson, A. D. Miranker and A. D. Hamilton, *Tetrahedron Lett.*, 2015, **56**, 3670–3673.

12 A. Smith, M. Guzman, P. Sprengeler, T. Keenan, R. Holcomb, J. Wood, P. Carroll and R. Hirschmann, *J. Am. Chem. Soc.*, 1994, **116**, 9947–9962.

13 J. T. Ernst, J. Becerril, H. S. Park, H. Yin and A. D. Hamilton, *Angew. Chem., Int. Ed.*, 2003, **42**, 535–539.

14 M. J. Adler, R. T. W. Scott and A. D. Hamilton, *Chem.–Eur. J.*, 2012, **18**, 12974–12977.

15 S. Thompson and A. D. Hamilton, *Org. Biomol. Chem.*, 2012, **10**, 5780–5782.

16 S. Thompson, R. Vallinayagam, M. J. Adler, R. T. W. Scott and A. D. Hamilton, *Tetrahedron*, 2012, **68**, 4501–4505.

17 J.-M. Ahn and S.-Y. Han, *Tetrahedron Lett.*, 2007, **48**, 3543–3547.

18 F. Lu, S.-W. Chi, D.-H. Kim, K.-H. Han, I. D. Kuntz and R. K. Guy, *J. Comb. Chem.*, 2006, **8**, 315–325.

19 H. Yin, G. Lee, K. A. Sedey, O. Kutzki, H. S. Park, B. P. Orner, J. T. Ernst, H.-G. Wang, S. M. Sebti and A. D. Hamilton, *J. Am. Chem. Soc.*, 2005, **127**, 10191–10196.

20 A. Raghuraman, E. Ko, L. M. Perez, T. R. Ioerger and K. Burgess, *J. Am. Chem. Soc.*, 2011, **133**, 12350–12353.

21 E. A. German, J. E. Ross, P. C. Knipe, M. F. Don, S. Thompson and A. D. Hamilton, *Angew. Chem., Int. Ed.*, 2015, **54**, 2649–2652.

22 T. Yamashita, P. C. Knipe, N. Busschaert, S. Thompson and A. D. Hamilton, *Chem.–Eur. J.*, 2015, **21**, 14699–14702.

23 B. B. Lao, I. Grishagin, H. Mesallati, T. F. Brewer, B. Z. Olenyuk and P. S. Arora, *Proc. Natl. Acad. Sci. U. S. A.*, 2014, **111**, 7531–7536.

24 L. Nevola, J. M. Rodrigeuz, S. Thompson and A. D. Hamilton, *Supramol. Chem.*, 2013, **25**, 586–590.

25 F. Bernardi, I. G. Csizmadia and A. Mangini, *Organic sulfur chemistry*, Elsevier Scientific Publishing Co., Amsterdam, 1985.

26 Y. Nagao, T. Hirata, S. Goto, S. Sano, A. Kakehi, K. Iizuka and M. Shiro, *J. Am. Chem. Soc.*, 1998, **120**, 3104–3110.

27 B. R. Beno, K.-S. Yeung, M. D. Bartberger, L. D. Pennington and N. A. Meanwell, *J. Med. Chem.*, 2015, **58**, 4383–4438.

28 The conformational control of the 1,5-S···O interaction was also observed in an alternative model system based on a thiophenylurea (ESI Fig. 2†).

29 *Maestro, version 10.2*, Schrödinger, LLC, New York, NY, 2015.

30 *Jaguar, version 8.8*, Schrödinger, LLC, New York, NY, 2015.

31 Y. Zhao and D. G. Truhlar, *Theor. Chem. Acc.*, 2007, **120**, 215–241.

32 W. J. Hehre, R. Ditchfield and J. A. Pople, *J. Chem. Phys.*, 1972, **56**, 2257–2261.

33 P. C. Hariharan and J. A. Pople, *Theor. Chim. Acta*, 1973, **28**, 213–222.

34 R. J. Woods, M. Khalil, W. Pell, S. H. Moffat and V. H. Smith, *J. Comput. Chem.*, 1990, **11**, 297–310.

35 T. Herz, R. Krauss, M. Kubbutat, M. Lang, C. Schaechtele, S. Tasler and F. Totzke, *US Pat.*, 7514460B2, 2009.

36 D. Neuhaus and M. P. Williamson, *The Nuclear Overhauser Effect in Structural and Conformational Analysis*, Wiley, 2nd edn, 2000.

37 For a discussion of the interpretation of peptidomimetic RMSD values see: D. Xin, L. M. Perez, T. R. Ioerger and K. Burgess, *Angew. Chem., Int. Ed.*, 2014, **53**, 3594–3598.

38 D. Eisenberg and M. Jucker, *Cell*, 2012, **148**, 1188–1203.

39 P. Cao, A. Abedini and D. P. Raleigh, *Curr. Opin. Struct. Biol.*, 2013, **23**, 82–89.

40 J. A. Williamson, J. P. Loria and A. D. Miranker, *J. Mol. Biol.*, 2009, **393**, 383–396.

41 C. A. De Carufel, N. Quittot, P. T. Nguyen and S. Bourgault, *Angew. Chem., Int. Ed.*, 2015, **54**, 14383–14387.

42 S. Kumar, D. E. Schlamadinger, M. A. Brown, J. M. Dunn, B. Mercado, J. A. Hebda, I. Saraogi, E. Rhoades, A. D. Hamilton and A. D. Miranker, *Chem. Biol.*, 2015, **22**, 369–378.

43 L. S. Wolfe, M. F. Calabrese, A. Nath, D. V. Blaho, A. D. Miranker and Y. Xiong, *Proc. Natl. Acad. Sci. U. S. A.*, 2010, **107**, 16863–16868.

44 An equimolar mixture of dioleoylphosphatidylglycerol (DOPG) and dioleoylphosphatidylcholine (DOPC) were extruded in to 100 nm vesicles.